Associating *IDH* and *TERT* Mutations in Glioma with Diffusion Anisotropy in Normal-Appearing White Matter

H. Halilibrahimoğlu, K. Polat, S. Keskin, O. Genç, O. Aslan, E. Öztürk-Işık, C. Yakıcıer, A.E. Danyeli, M.N. Pamir, K. Özduman, A. Dinçer, and A. Özcan

ABSTRACT

BACKGROUND AND PURPOSE: *IDH* and *TERT* mutations might infiltratively manifest within normal-appearing white matter with specific phenotypes such as microstructural changes undetectable by standard MR imaging contrasts but potentially associable with DTI variables. The aim of this retrospective glioma study was to statistically investigate *IDH* and *TERT* associations and classifications with DTI reported microstructure in normal-appearing white matter.

MATERIALS AND METHODS: Retrospective data from patients imaged between March 2012 and February 2016 were analyzed by grouping them as *IDH–TERT* subgroups and by *IDH* and *TERT* mutation status. DTI variables in the *IDH-TERT* subgroups were first identified by the Kruskal-Wallis test, followed by Dunn-Šidák multiple comparisons with Bonferroni correction. *IDH* and *TERT* mutations were compared with the Mann-Whitney U test. Classification by thresholding was tested using receiver operating characteristic analysis.

RESULTS: Of 170 patients, 70 patients (mean age, 43.73 [SD, 15.32] years; 40 men) were included. Whole-brain normal-appearing white matter fractional anisotropy (FA) and relative anisotropy (RA) ($P = .002$) were significantly higher and the contralateral-ipsilateral hemispheric differences, ΔFA and ΔRA, ($P < .001$) were significantly lower in IDHonly patients compared with TERTonly, with a higher whole-brain normal-appearing white matter FA and RA ($P = .01$) and ΔFA and ΔRA ($P = .002$) compared to double positive patients. Whole-brain normal-appearing white matter ADC ($P = .02$), RD ($P = .001$), λ_2 ($P = .001$), and λ_3 ($P = .001$) were higher in *IDH* wild-type. Whole-brain normal-appearing white matter λ_1 (AD) ($P = .003$), FA ($P < .001$), and RA ($P = .003$) were higher, but $\Delta\lambda_1$ ($P = .002$), ΔFA, and ΔRA ($P < .001$) were lower in *IDH* mutant versus *IDH* wild-type. ΔFA ($P = .01$) and ΔRA ($P = .02$) were significantly higher in *TERT* mutant versus *TERT* wild-type.

CONCLUSIONS: Axial and nonaxial diffusivities, anisotropy indices in the normal-appearing white matter and their interhemispheric differences demonstrated microstructural differences between *IDH* and *TERT* mutations, with the potential for classification methods.

ABBREVIATIONS: AD = axial diffusivity; AUC = area under the curve; DAI = diffusion anisotropy indices; DN = double negative; DP = double positive; FA = fractional anisotropy; HMeD = hemispherical mean differences; LBTh = lower bound thresholding; mut = mutant; NAWM = normal-appearing white matter; NPV = negative predictive value; PPV = positive predictive value; RA = relative anisotropy; RD = radial diffusivity; ROC = receiver operating characteristic; UBTh = upper bound thresholding; WB = whole brain; wt = wild-type

G lioma is the most common CNS tumor with overall survival ranging from 12 to 15 months to several years, depending on tumor severity.[1] Recently, genotype information in clinical workflow proved to be valuable[2] and was integrated into the WHO classification.[3] Therein, *isocitrate dehydrogenase* (*IDH*) mutation is associated with longer overall survival, around 57 months, and is commonly seen in low-grade (grade 2, grade 3) gliomas.[2,4-6] *Telomerase reverse transcriptase* (*TERT*) mutation presents with a more aggressive disease course, eg, with neutrophil infiltration,[7] leading to a lower overall survival of 11.5 months, mostly in high-grade (grade 4) tumors.[2,8] Remarkably, overall survival increases to 125 months when the tumor is both *IDH*- and *TERT*-mutated.[6]

FIG 1. Patient-selection flowchart.

Table 1: Cohort characteristics

Patient Demographics (*n* = 70)	
Mean age (yr)	43.73 (SD, 15.32)
Sex (female/male)	30/40
Tumor characteristics	
Mutation status wt/mut (No.) (%)	
IDHmut	29/41 (41%/59%)
TERTmut	33/37 (47%/53%)
Tumor grade, mutation (No.) (%)	
1, IDHmut/TERTmut	1 (1%), 0/0
2, IDHmut/TERTmut	29 (41%), 24/16
3, IDHmut/TERTmut	22 (31%), 15/8
4, IDHmut/TERTmut	18 (26%), 2/13

When identifying genotypes, biopsy might miss relevant loci due to the notorious heterogeneity of gliomas.[9] Complete organ coverage by MR imaging might provide a more accurate assessment, especially by analyzing the normal-appearing white matter (NAWM) for the diffuse properties of the disease such as infiltrative tendencies to migrate through white matter fibers.[10,11]

The migration process involves complex interactions with extracellular matrix components and cytokines, which, in turn, lead to displacement or, for grade 4, destruction of the white matter fibers.[12] T1WI and T2WI might not be sufficiently sensitive to NAWM infiltration,[13] whereas microstructural changes such as neoplastic angiogenesis and elevated cellular density[14,15] are investigated with DTI and quantified by its eigenvalues and diffusion anisotropy indices (DAIs).[16]

In the past, decreased relative anisotropy (RA) found in the NAWM of patients with high-grade gliomas,[17] and increased ADC coupled with decreased *N*-acetylaspartate in the contralateral NAWM suggested microstructural damage possibly caused by infiltrating tumor cells.[18] Tumor grades histopathologically report microstructure;[19] so low-grade and, therefore, *IDH* mutated (IDHmut) tumors exhibit higher diffusion anisotropy and lower ADC in the NAWM compared with high-grade[17,20] and *IDH* wild-type (wt)[21] tumors. In addition, DAI changes in the distal NAWM have been reported for different glioma grades.[22]

Complementing tumor-site-focused past studies by investigating regions outside the tumor might potentially be relevant because it would inform on the diffuse nature of the disease. The aim of this study was to investigate microstructural changes in the NAWM by analyzing comprehensively the DTI variables within the whole brain (WB) and between "healthy" and "pathologic" hemispheres, for statistically associating them with *IDH* and *TERT* mutations.

MATERIALS AND METHODS
Clinical Data
In this institutional review board–approved retrospective study, the cohort was gathered without recruitment from existing data of clinical patients who had consented. Of 170 consecutive patients with gliomas treated at Acıbadem Hospitals (Istanbul, Turkey) between March 2012 and February 2016, with written informed consent, 54 without T2WI and/or DTI, 30 postoperative, 2 with unavailable mutation data and 11 with unavailable TERT status, 2 with conflicting genetic results, and 1 with a suboptimal NAWM DTI mask were excluded (Fig 1), leaving 70 patients (mean age, 43.73 [SD, 15.32] years of age; female/male ratio: 30/40), with 1 grade 1, 29 grade 2, 22 grade 3, and 18 grade 4 gliomas and 41 patients with IDHmut (29 IDHwt); 37 patients were TERTmut (33 TERTwt).

Histopathologic analysis was performed on surgically removed tumor samples. *IDH* and *TERT* mutations were determined using either minisequencing or Sanger sequencing. Patients were stratified into 4 molecular subgroups, hereafter referred to as *IDH-TERT* subgroups (Table 1):

1) Double negative (DN): IDHwt, TERTwt (*n* = 9).
2) IDHonly: IDHmut, TERTwt (*n* = 24).
3) TERTonly: IDHwt, TERTmut (*n* = 20).
4) Double positive (DP): IDHmut, TERTmut (*n* = 17).

MR Imaging Data
MR imaging was performed on a 3T Magnetom Tim Trio MR imaging scanner (Siemens) with a 32–channel head coil, 1–7 days before the operation. The scanning protocol included T2WI acquired using a 2D turbo spin-echo sequence with voxel dimensions of $0.26 \times 0.26 \times 0.26$ mm with 20 axial slices, TE/TR = 107/3470 ms, slice thickness/spacing = 5/6.5 mm, flip angle = 120°. DTI data were acquired using a 2D diffusion EPI sequence with $1.8 \times 1.8 \times 1.8$ mm voxels, 60 axial slices, TE/TR = 107/3470 ms, slice thickness/spacing = 1.8/2.34 mm, flip angle = 90°, and b-value = 1000 ms/mm^2 with 20 diffusion gradient vectors. Eigenvalue maps for the 3 eigenvalues ($\lambda_1 \geq \lambda_2 \geq \lambda_3$) were computed by the console computer of the scanner.
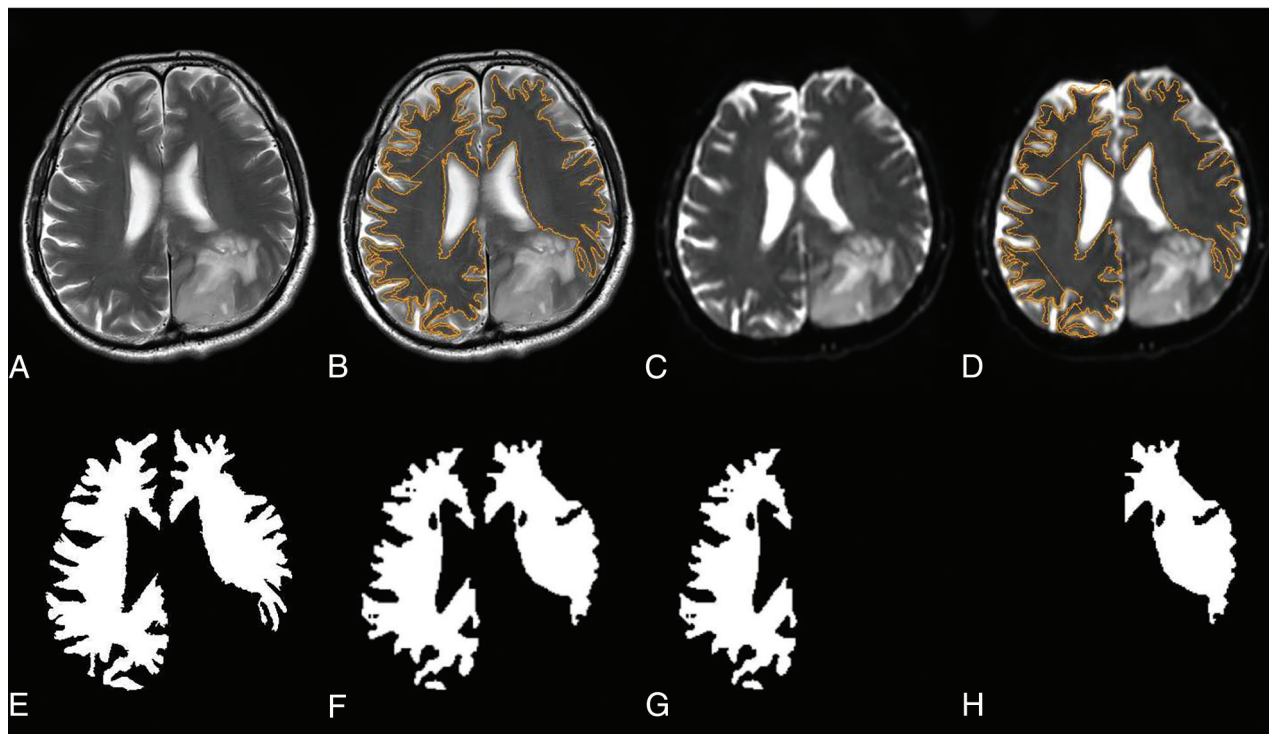
FIG 2. NAWM segmentations and masks. T2WI (*A*), semiautomatic NAWM boundary demarcations overlaid on T2WI (*B*), the coregistered B_0 image (*C*), NAWM boundary demarcations on the coregistered B_0 image (*D*), total NAWM mask on T2WI (*E*), on B_0 image (*F*), and the corresponding right (*G*) and left (*H*) hemisphere masks.

All image volumes were transferred in DICOM format, then anonymized using in-house-developed scripts based on the Grassroots DICOM library[23] and were converted to Neuroimaging Informatics Technology Initiative (NIfTI) format using Medical Image Processing, Analysis, and Visualization software (MIPAV; http://mipav.cit.nih.gov).[24]

NAWM Segmentation and Coregistration

NAWM regions were selected on T2WI using semiautomatic level set segmentation tools in MIPAV by 2 trainees with 2 years of experience OG and OA, inspected by an imaging scientist with 25+ years of experience AÖ, and approved by a neuroradiologist with 30+ years of experience, AD.

Images obtained without diffusion weighting (B_0 images) were coregistered onto T2WI with the FSL software package (http://www.fmrib.ox.ac.uk/fsl)[25] using the mutual information cost function with the trilinear interpolation method. The transformation optimizing the $B_0 \rightarrow$T2WI coregistration problem was applied for coregistering eigenvalue maps onto T2WI by interpolating with the nearest neighbor method (Fig 2).

The distortion of NAWM masks caused by the difference of total slice numbers among the MR imaging modalities while coregistering was corrected with an in-house-developed Matlab (MathWorks) code (KP, 2+ years of experience), which identifies shared pixel coordinates in matching B_0 images mapped to T2WI and the original B_0 image. The code infers mask pixels in the "sandwich" slices from the "shell" slices.

Furthermore, an in-house-developed (KP, 2+ years of experience) Matlab code subdivided the mask images automatically into left and right hemispheres, which were used for computing contralateral and ipsilateral DAI and eigenvalue distributions (Fig 2). Quality assurance for the image-processing routines was conducted by HH, SK and KP, each with 2+ years of experience, and inspected and approved as aforementioned.

Variables

For each patient, DAIs (Online Supplemental Data) were computed from the eigenvalues ($\lambda_1 \geq \lambda_2 \geq \lambda_3$) on WB, contralateral, and ipsilateral NAWM pixels. For each patient, each variable's mean over WB, $Mean_{WB}$, and the hemispheres, $Mean_{contralat}$, $Mean_{ipsilat}$, were calculated. Each patient's ipsilateral hemisphere mean was subtracted from the contralateral hemisphere mean for obtaining in-patient hemispherical mean differences (HMeD) of DAIs and eigenvalues:

$$HMeD(I) = \Delta I = Mean_{contralat}(I) - Mean_{ipsilat}(I),$$

where I denotes any of the DTI variables. All of the computations were implemented with in-house-developed Matlab code (HH, 2+ years of experience).

Statistical Analysis

Statistical power calculations indicate that with the exception of ADC, whose results were nevertheless reported herein, all of the variables had acceptable statistical power for the number of included patients (Online Supplemental Data).

The Kruskal-Wallis test with a $P < .05$ threshold was used for testing whether DAIs and eigenvalues could detect differences among *IDH-TERT* subgroups. Variables with statistical significance were then subjected to a Dunn–Šidák multiple comparison analysis with pair-wise subgroup comparisons for identifying differentiating variables. Subsequently, *P* values of multiple comparison analysis

Table 2: Comparison of WB-NAWM means and HMeD of diffusion parameters for *IDH-TERT* molecular subgroups

	ADC	λ_1 (AD)	RD	λ_2	λ_3	FA	RA
IDH-TERT subgroup Kruskal-Wallis test *P* values							
WB–NAWM	.10	.03[a]	.01[a]	.01[a]	.01[a]	.001[a]	.001[a]
HMeD	.10	.01[a]	.04[a]	.044[a]	.02[a]	<.001[a]	<.001[a]
IDH-TERT subgroup multiple comparisons *P* values							
WB-NAWM							
DN vs IDHonly	–	.59	.64	.61	.74	.52	.58
DN vs TERTonly	–	.99	.87	.88	.86	.82	.77
DN vs DP	–	.70	.82	.91	.79	.68	.69
IDHonly vs TERTonly	–	.04[a]	.01[b]	.007[b]	.01[a]	.002[b]	.002[b]
IDHonly vs DP	–	>.99	>.99	.99	>.99	>.99	>.99
TERTonly vs DP	–	.10	.04[a]	.08	.03[a]	.01[a]	.01[a]
HMeD							
DN vs IDHonly	–	.02[a]	.61	.26	.99	.86	.79
DN vs TERTonly	–	.89	.04[a]	.04[a]	.06	.21	.30
DN vs DP	–	.25	.91	.75	>.99	.96	.89
IDHonly vs TERTonly	–	.07	.44	.87	.07	<.001[b]	<001[b]
IDHonly vs DP	–	.87	>.99	.96	>.99	>.99	>.99
TERTonly vs DP	–	.75	.22	.41	.08	.002[b]	.002[b]

Note:—En dash indicates that multiple comparisons were not performed due to lack of statistical significance in the Kruskal-Wallis test.
[a] $P < .05$.
[b] $P < .008$.

eigenvalues ($P < .05$), with the exception of ADC ($P = .10$ for WB–NAWM ADC) (Table 2). In pair-wise *IDH-TERT* subgroup comparisons, WB-NAWM radial diffusivity (RD) was higher in TERTonly patients compared to IDHonly ($P = .01$), with higher values in TERTonly compared to DP patients ($P = .04$) (Fig 3). WB-NAWM fractional anisotropy (FA) and RA were significantly higher in IDHonly patients compared to TERTonly ($P = .002$ for both), with a higher WB-NAWM FA and RA compared to DP ($P = .01$ for both). WB-NAWM axial diffusivity (AD) had higher values in the IDHonly subgroup compared with TERTonly ($P = .04$), whereas WB-NAWM λ_2 had significantly higher values ($P = .007$) and WB-NAWM λ_3 showed higher values ($P = .01$) in the TERTonly gliomas compared to IDHonly. WB-NAWM λ_3 also had higher values in TERTonly patients compared to DP ($P = .03$).

were adjusted with the Bonferroni correction ($P < .008$). Anisotropy differences between *IDH* and *TERT* mutation status were compared using the Mann-Whitney *U* test with a threshold of $P < .05$.

Statistical analysis was performed with Matlab Statistics and Machine Learning Toolbox (https://www.mathworks.com/products/statistics.html) by HH under the supervision of AÖ with 6+ and 25+ years of experience, respectively.

Classification by Thresholding

For investigating genotype classification as proof of principle, decision by thresholding was tested on each variable for separating each mutation group from the rest. Classifier performance was investigated with the receiver operating characteristic[26] (ROC) curve's area under the curve (AUC)[26] (with AUC = 1 as the best performance indicator) and positive and negative predictive values (PPV, NPV) at the optimal operating threshold identified by determining on each ROC curve the closest point to the top left corner (False Positive Rate = 0, True Positive Rate = 1), corresponding to sensitivity = 1 and specificity = 1 (Online Supplemental Data).

The steps were applied using each threshold as a lower bound (Value ≥ Threshold) and as an upper bound (Value ≤ Threshold). Therein, AUC values for these decision criteria add up to 1, leading to select the thresholding criterion (upper or lower bound) with a higher AUC for a given variable. By contrast, an AUC close to 0.5 indicates poor classification capability of the variable (Online Supplemental Data).

ROC analysis and reporting were implemented with in-house Matlab code developed by AÖ with 25+ years of experience.

RESULTS
IDH–TERT Subgroups
Whole Brain. Among *IDH-TERT* subgroups, in the WB-NAWM, there was a statistically significant difference in all DAIs and

Interhemispheric Differences. When comparing hemispheres within *IDH-TERT* subgroups, there was a statistically significant difference in the interhemispheric mean differences of all DAIs and eigenvalues ($P < .05$), with the exception of ADC ($P = .10$ for ΔADC) (Table 2). With the exception of DN and DP groups, ΔADC distributions completely shifted to negative values, indicating that in the presence of only a single mutation, ADC values on the "healthy" (contralateral) side tend to be lower than those of the tumor (ipsilateral) side.

For all *IDH-TERT* subgroups, λ_2, λ_3, and thus RD had larger values ipsilaterally. TERTonly had the largest shift, followed by IDHonly. HMeD medians in DN and DP were negative but closer to zero. With the exception of λ_1 (AD) of the DN, all the diffusivities had higher values ipsilaterally for the *IDH-TERT* subgroups. This finding might potentially indicate an overall disruption of the microstructure in the tumor hemisphere.

For TERTonly and DP, the median of $\Delta\lambda_1$ was negative but closer to zero, indicating a higher λ_1 ipsilaterally. $\Delta\lambda_1$ was lower in IDHonly gliomas compared to DN ($P = .02$). DN and TERTonly distributions point to higher contralateral anisotropy significantly in TERTonly and mildly in DN. ΔRD and $\Delta\lambda_2$ had higher values in DN patients in comparison to TERTonly ($P = .04$ for both).

Distributions of ΔFA and ΔRA from IDHonly and DP had median values close to zero, indicating anisotropy resemblance of the hemispheres for these mutations. ΔFA and ΔRA were significantly higher in TERTonly gliomas compared to IDHonly ($P < .001$ for both) and DP ($P = .002$ for both) (Fig 4 and Table 2). Lastly, distributions of DN and TERTonly point to higher contralateral anisotropy significantly in TERTonly and mildly in DN.

IDH and TERT Mutation Status
Whole Brain. Among IDHwt and IDHmut gliomas, WB-NAWM ADC ($P = .02$), RD ($P = .001$), λ_2 ($P = .001$), and λ_3 ($P = .001$)

WHOLE-BRAIN NAWM
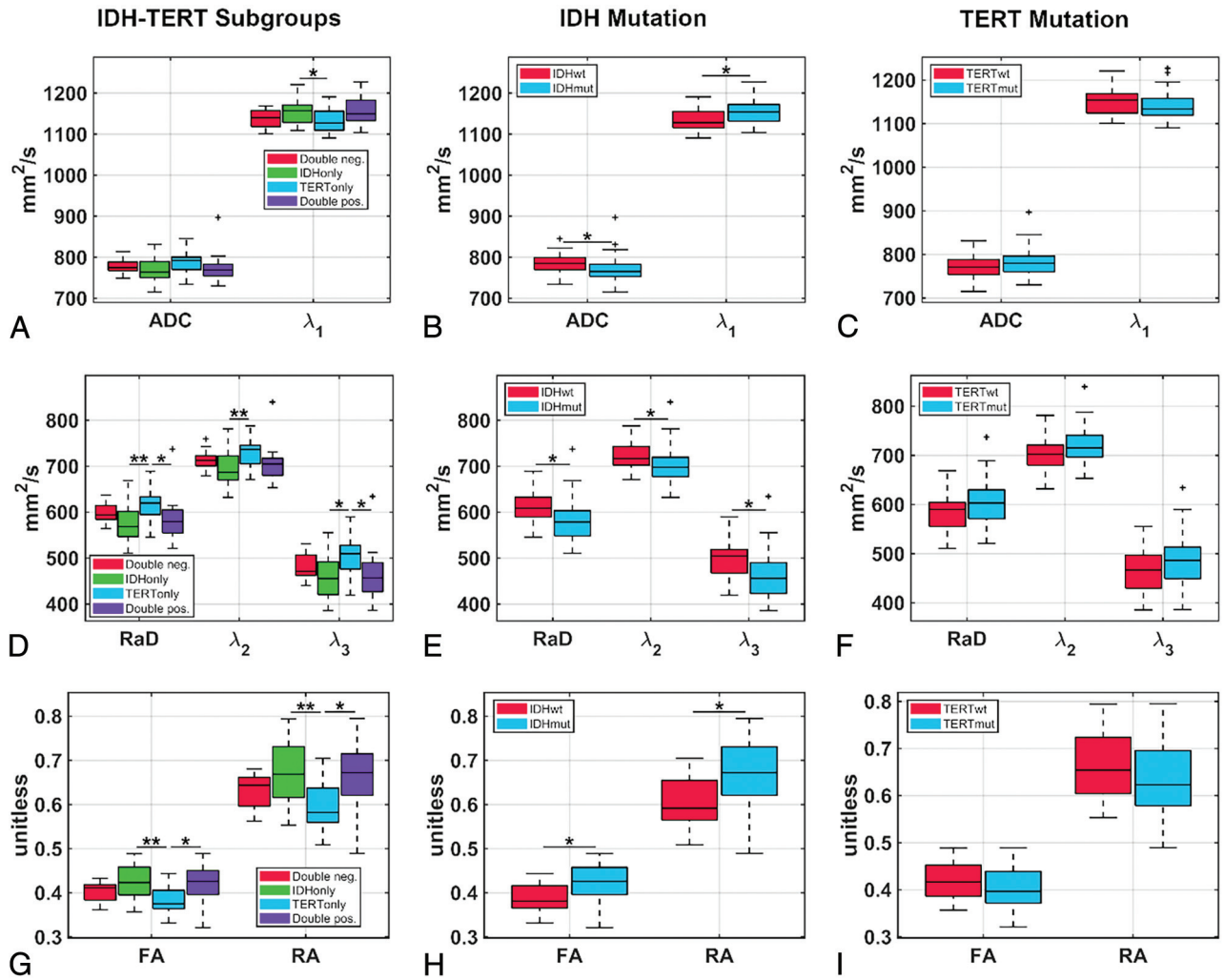
FIG 3. Boxplots of WB-NAWM means of ADC, λ_1, RD, λ_2, λ_3, FA, and RA grouped by *IDH-TERT* subgroups (*A*), *IDH* mutation (*B*), and *TERT* (*C*) mutation statuses, respectively. The *asterisk* indicates $P < .05$, and *double asterisks* indicate $P < .008$ according to the Bonferroni correction for multiple-comparison analysis. The *plus sign* indicates outlier values, *whiskers* indicate minimum and maximum values, the *box limits* are 25th and 75th percentiles, and the *midline* shows the median. Neg. indicates negative; pos., positive.

were higher in the IDHwt group (Table 3). In contrast, WB-NAWM λ_1 ($P = .003$), FA ($P < .001$), and RA ($P = .003$) were higher in IDHmut gliomas compared to IDHwt.

When TERTwt and TERTmut gliomas were compared, none of the WB-NAWM DAIs and eigenvalues demonstrated a statistically significant difference ($P > .05$).

In consequence, similar relative median levels presented in all of the variables when comparing IDHwt and TERTmut versus their respective counterparts (eg, lower AD and higher RD for IDHwt and TERTmut versus IDHmut and TERTwt, respectively) demonstrated a common phenotype for these aggressive genotypes.

Interhemispheric Differences. For wild-type and mutant pairs, all of the diffusivity variables for all of the genotype pairs showed higher values ipsilaterally. ΔADC, ΔRD, and $\Delta\lambda_2$ were leveled; $\Delta\lambda_1$ differed more for IDHmut and TERTwt, and, likewise, $\Delta\lambda_3$ for IDHwt and TERTmut. IDHmut and TERTwt did not show interhemispheric difference for any anisotropy index, whereas

IDHwt and TERTmut had higher values contralaterally for RA and FA.

ΔFA, ΔRA ($P < .001$ for both), and $\Delta\lambda_1$ ($P = .002$) were higher in the IDHwt group compared to IDHmut. ΔADC ($P = .48$), ΔRD ($P = .32$), $\Delta\lambda_2$ ($P = .73$), and $\Delta\lambda_3$ ($P = .055$) had no statistically significant difference among IDH mutation statuses.

With a remarkable resemblance, ΔFA ($P = .01$) and ΔRA ($P = .02$) were higher in TERTmut patients compared to TERTwt. ΔADC ($P = .73$), $\Delta\lambda_1$ ($P = .31$), ΔRD ($P = .14$), $\Delta\lambda_2$ ($P = .27$), and $\Delta\lambda_3$ ($P = .054$) had no statistically significant difference among TERT mutation statuses.

Classification by Thresholding
Numeric results in this section are fully presented in the Online Supplemental Data.

IDH-TERT **Subgroups.** For WB-NAWM, the best PPV was obtained for TERTonly by FA and RA (0.6842 for both) with
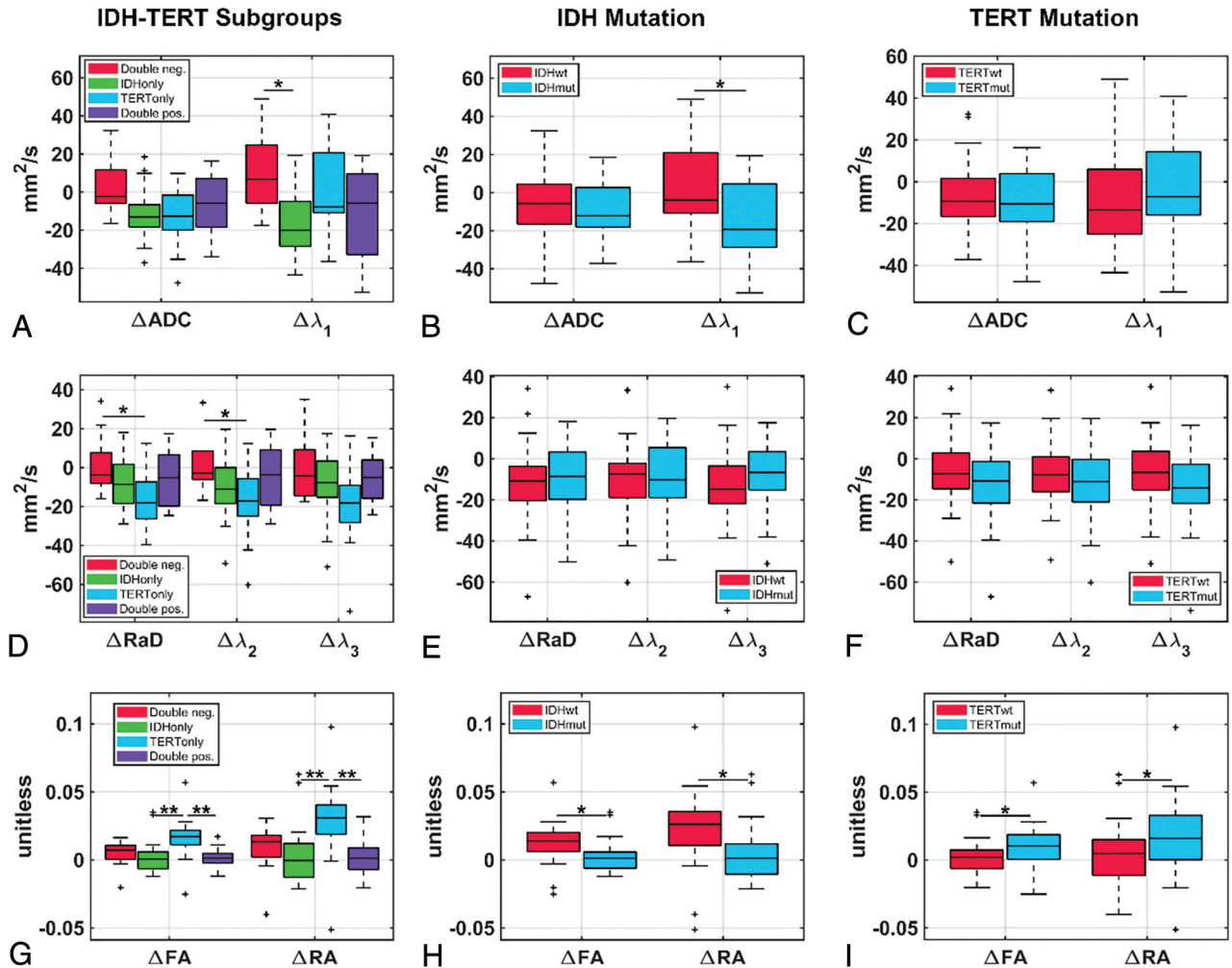
HEMISPHERE DIFFERENCE NAWM

FIG 4. Boxplots of HMeD (contralateral-ipsilateral) of ADC, λ_1, RD, λ_2, λ_3, FA, and RA grouped by *IDH-TERT* subgroups (*A*), *IDH* mutation (*B*), and *TERT* mutation (*C*) statuses, respectively. Fig 3 and Fig 4 legends are the same.

upper bound thresholding (UBTh); overall, PPVs were low (minimum 0.1429 DN with RA lower bound thresholding [LBTh], and 0.1464 DN ADC with UBTh). In contrast, NPVs had higher values with the highest from 0.9355 for DN with RD LBTh. DN had higher NPVs for all variables for LBTh and UBTh, followed by DP, TERTonly, and IDHonly (Online Supplemental Data).

AUC values from WB-NAWM reported TERTonly classification as the best for RA (0.7800), FA (0.7760), and λ_1 (AD) (0.7030) with UBTh and RD (0.7470), λ_3 (0.7460), λ_2 (0.7400), and ADC (0.670) with LBTh. DN had the worst performance with AUC values close to 0.5, which was also supported by the poor PPV performance for LBTh. λ_1 (AD), FA, and RA had above-average performance on IDHonly and DP using LBTh (Online Supplemental Data).

The WB-NAWM findings are aligned with the results of the "Whole Brain" section of the "*IDH-TERT* Subgroups" section. Overall poor classification performance on DN agreed with its lack of a statistically significant difference from the other groups. FA and RA, which showed the most statistically significant differences among subgroups, especially for TERTonly classification (Fig 3A,-D, -G), had the best classifier performances.

Interhemispheric differences had poor PPVs for LBTh with the highest 0.7895 for ΔRA on TERTonly followed by 0.6296 for ΔFA on TERTonly, then followed by a substantial drop to 0.4324. For UBTh, ΔRA provided for TERTonly PPV = 1; however, the second highest value was 0.5667, which is a significant drop reflecting on overall performance. Interhemispheric NPVs had much higher values over different variables and genotypes, and higher values were concentrated on DN (maximum = 0.9750 from ΔADC and $\Delta\lambda_2$ for LBTh; maximum = 0.9167 from ΔFA for UBTh), presenting with high values overall (minimum = 0.5750 for LBTh, 0.6304 for UBTh) (Online Supplemental Data).

Interhemispheric differences demonstrated the best AUC values on TERTonly from ΔFA (0.8330) and ΔRA (0.8280) with LBTh. DN has good performance for $\Delta\lambda_1$ (ΔAD) (0.7377), ΔADC (0.7341), $\Delta\lambda_2$ (0.7341), and ΔRD (0.7013) with LBTh. Performance on DP and IDHonly was poor with the exception of ΔFA (DP: 0.6349, IDHonly: 0.6902) and ΔRA (DP: 0.6448, IDHonly: 0.6866) performing better for both, and $\Delta\lambda_1$ (ΔAD) (0.6975), for IDHonly (Online Supplemental Data), all using UBTh.

For interhemispheric differences, good performance of ΔFA and ΔRA for the TERTonly classification was in line with the

Table 3: Comparison of WB–NAWM means and HMeD of diffusion parameters for *IDH* and *TERT* mutation status

	ADC	λ_1 (AD)	RD	λ_2	λ_3	FA	RA
IDHmut Mann-Whitney test P values							
WB–NAWM	.02[a]	.003[a]	.001[a]	.001[a]	.001[a]	<.001[a]	.03[a]
HMeD	.48	.002[a]	.32	.73	.055	<.001[a]	<.001[a]
TERTmut Mann-Whitney test P values							
WB–NAWM	.21	.22	.09	.057	.12	.07	.07
HMeD	.73	.31	.14	.27	.054	.01[a]	.02[a]

[a] $P < .05$.

results of the "Interhemispheric Differences" section under the "RESULTS" section (Fig 4G), while AUC values of ΔADC, ΔAD, ΔRD, and $\Delta\lambda_2$ for classifying DN aligned with the separation of DN from the other subgroups in Fig 4A, -D.

IDH and *TERT* Mutation Status. For WB-NAWM, PPVs were higher compared with NPVs. The highest PPV (0.7714) was obtained with LBTh of FA on IDHmut followed by λ_1 (AD) (0.7500) and RA (0.7381), while λ_2 (0.7647), RD (0.7632), ADC (0.7576), and λ_3 (0.7568) also performed well using UBTh. PPVs for the TERTmut classification were modest with RD (0.6897) and FA (0.4828) providing maximum and minimum PPVs for LBTh, and λ_1 (AD) (0.6563) and λ_2 (0.4545), for UBTh. NPVs, on the other hand, had poor values with maximum values from RA (0.6429) using LBTh and RD (0.6250) using UBTh for IDHmut, and λ_3 (0.5882) using LBTh and FA (0.5833) using UBTh for TERTmut, with minimum values from RD (0.3333) using LBTh and RA (0.2778) using UBTh for IDHmut, and RA (0.4359) using LBTh and λ_2 (0.4054) using UBTh for TERTmut (Online Supplemental Data).

AUC values from WB-NAWM indicated good performance for IDHmut: FA and RA (0.7653 both) and λ_1 (AD) (0.7115) for LBTh, and RD (0.7359), λ_3 (0.7325), and λ_2 (0.7283) for UBTh. In contrast, TERTmut had mediocre performance with λ_2 (0.6331), RD (0.6200), and λ_3 (0.6077) using LBTh and FA (0.6282) and RA (0.6274) using UBTh (Online Supplemental Data).

The better classifier performance of WB-NAWM on IDHmut was in line with its statistically significant difference from IDHwt present for all variables, shown in Fig 3B, -E, -H, whereas the lack of statistical significance for TERTmut depicted in Fig 3C, -F, -I reflected a mediocre classifier performance.

Interhemispheric difference PPVs had the highest values for IDHmut with ΔAD (0.8519), ΔFA (0.8250), and ΔRA (0.8158) using UBTh which agrees with Fig 4A–H where the IDHmut distributions for the aforementioned variables lie below the IDHwt distributions. These variables also had statistically significant differences. The highest PPV for TERTmut occurred for ΔRA (0.8182) followed by ΔFA (0.7778), both using LBTh, in accordance with Fig 4I, where the ΔFA and ΔRA distributions of TERTmut were placed slightly higher than TERTwt distributions; also, ΔFA and ΔRA were the only variables presenting a statistically significant difference (Fig 4C, -F, -I).

IDHmut NPVs for ΔFA and ΔRA were both equal to 1 for LBTh, which was in accordance with Fig 4H where IDHmut ΔFA and ΔRA distributions were below IDHwt distributions and presented statistically significant differences. However, the remaining

NPVs were all below 0.5625 ($\Delta\lambda_3$). The highest NPVs for TERTmut were all from LBTh for ΔAD (0.6333), ΔFA (0.6279), and ΔRA (0.6042), with ΔFA and ΔRA being the only variables with statistically significant differences in Fig 4C, -F, -I.

The AUC classifier performance agreed with the predictive value and statistical findings: ΔRA (0.7830), ΔFA (0.7788), and ΔAD (0.7149) had the best values for IDHmut all using UBTh; likewise, the best AUC values of TERTmut were ΔFA (0.6732), ΔRA (0.6618), and ΔAD (0.5717) all using LBTh.

DISCUSSION

In this study, DTI variables from the WB-NAWM of patients with gliomas and their interhemispheric differences were investigated for their association with *IDH-TERT*–based genotypes. DTI variables were analyzed as indicators of microstructural integrity in the NAWM for associating them as phenotypes of the mutations.

By probing the diffuse nature of the disease, which was scarcely studied in the past, this investigation complemented the studies focusing solely on the tumor region characteristics. In fact, there are very few glioma NAWM investigations with limited basis and scope: limited coverage of NAWM, relating interhemispheric FA differences to neurometabolites with contralateral FA increase,[27] positively correlating ADC to tumor grades,[22] and suggesting radiation-induced fiber damage for reducing interhemispheric FA difference.[28] In contrast, for this study, NAWM data were obtained comprehensively from the WB, the hemispheres, and interhemispheric computations for radiogenomics analysis.

First, while lacking statistical significance in this study, if AD and λ_2 can also differentiate between TERTonly and DP for a larger cohort in the future, DTI variables might be considered as markers separating TERTonly from groups containing IDHmut.

In aggressive gliomas, ie, IDHwt and its subset TERTonly, WB-NAWM exhibited higher ADC. However, this observation does not necessarily grant a relevance to WB-NAWM ADC due to the canceling by AD and nonaxial diffusivities when computing ADC as their sum. Nevertheless, in the literature, NAWM ADC increase in patients with IDHwt has been related to vasogenic edema and tumor infiltration–related tissue damage.[18,29,30] Our results for IDHmut matched those in a recent study that showed lower NAWM FA and higher NAWM ADC and RD in IDHwt versus IDHmut,[21] but a decrease in AD reported therein contradicts our observations. This issue potentially stems from using the analysis variable FA in the skeletonization algorithm[31] for NAWM masking in Jütten et al[21] versus our comprehensive nonselective NAWM masking.

Taking the AD and RD are markers for axonal integrity,[32] in agreement with the findings of this study, a decrease in AD and FA and an increase in RD after radiation therapy were reported as resulting from radiation–related NAWM damage.[33] A recent study found lower FA, and AD as well as higher ADC and RD in regions with high tumor infiltration.[34] Furthermore, histopathologic studies also agree with higher ADC and lower FA of more

aggressive genotypes, suggesting tumor infiltration–related damage with increasing infiltration.[35,36] This also agrees with the observation where lower FA and RA for TERTonly indicate a tendency for molecular-motion isotropy in the WB-NAWM. However, pinpointing the microstructural changes behind the observations reported herein, especially in *TERT* subgroups, requires further histopathologic investigations.

In the IDHonly group, mostly negatively valued ΔAD distribution showed that AD tends to be larger on the ipsilateral side, arguing that the deformation/pressure caused by the tumor might be pushing the molecular motion in the direction of the major axis of the microstructure. In contrast, in the DN subgroup, the contralateral side tended to have larger AD, accordingly, ΔAD differentiates between only DN and IDHonly. Without notable physical deformation in the contralateral side, the causes behind major axis directional preference in groups with IDHwt are an open problem.

The interhemispheric observations, especially in aggressive genotypes such as IDHwt and TERTmut, including TERTonly, suggest that molecular motion was more isotropic in the ipsilateral hemisphere, potentially indicating loss of microstructural integrity therein. This suggestion agrees with findings in previous studies of decreasing microstructural organization in distal NAWM near the tumor.[27] The observation in more aggressive genotypes may link the increased NAWM damage to higher-grade tumors where IDHwt and TERTmut genotypes are more prevalent.[22]

This investigation was limited by a construct of its methodology. Summarizing the properties of large ROIs such as the WB or the hemispheres with a single number, ie, the mean, is suitable for statistical analysis but limits their rich information content. Differing distributions from different patients might have the same mean, which raises the concern of hampering classification and thereby genotype prediction when the ROI means are used as features. By contrast, the full properties of distributions might better characterize microstructural phenotypes associated with the mutations, resulting in more accurate prediction thereof.

CONCLUSIONS

For NAWM, statistical analysis indicated that axial and nonaxial diffusivities, anisotropy indices, and interhemispheric differences proved to be the most associating variables for subgroups of *IDH* and *TERT* mutations. Additionally, the most basic classification methodology, ie, thresholding, provided optimistic classification performance despite its shortcoming as an one dimensional decision criterion. In the future, full distributions of the DTI variables from the WB, hemispheres, and their interhemispheric differences should be analyzed with machine learning methods for fully taking advantage of their richer information content residing in high-dimensional data spaces.

ACKNOWLEDGMENTS

REFERENCES

1. Ostrom QT, Patil N, Cioffi G, et al. **CBTRUS Statistical Report: primary brain and other central nervous system tumors diagnosed in the United States in 2013–2017**. *Neuro Oncol* 2020;22:iv1–96 CrossRef Medline
2. Eckel-Passow JE, Lachance DH, Molinaro AM, et al. **Glioma groups based on 1p/19q, IDH, and TERT promoter mutations in tumors**. *N Engl J Med* 2015;372:2499–508 CrossRef Medline
3. Louis DN, Perry A, Wesseling P, et al. **The 2021 WHO Classification of Tumors of the Central Nervous System: a summary**. *Neuro Oncol* 2021;23:1231–51 CrossRef Medline
4. Parsons DW, Jones S, Zhang X, et al. **An integrated genomic analysis of human glioblastoma multiforme**. *Science* 2008;321:1807–12 CrossRef Medline
5. Brat DJ, Verhaak RG, Aldape KD, et al; Cancer Genome Atlas Research Network. **Comprehensive, integrative genomic analysis of diffuse lower-grade gliomas**. *N Engl J Med* 2015;372:2481–98 CrossRef Medline
6. Killela PJ, Pirozzi CJ, Healy P, et al. **Mutations in IDH1, IDH2, and in the TERT promoter define clinically distinct subgroups of adult malignant gliomas**. *Oncotarget* 2014;5:1515–25 CrossRef Medline
7. Gao M, Lin Y, Liu X, et al. **TERT mutation is accompanied by neutrophil infiltration and contributes to poor survival in isocitrate dehydrogenase wild-type glioma**. *Front Cell Dev Biol* 2021;9:654407 CrossRef Medline
8. Colebatch AJ, Dobrovic A, Cooper WA. **TERT gene: its function and dysregulation in cancer**. *J Clin Pathol* 2019;72:281–84 CrossRef Medline
9. Barbaro M, Fine HA, Magge RS. **Scientific and clinical challenges within neuro-oncology**. *World Neurosurg* 2021;151:402–10 CrossRef Medline
10. Sahm F, Capper D, Jeibmann A, et al. **Addressing diffuse glioma as a systemic brain disease with single-cell analysis**. *Arch Neurol* 2012;69:523–26 CrossRef Medline
11. Esmaeili M, Stensjøen AL, Berntsen EM, et al. **The direction of tumour growth in glioblastoma patients**. *Sci Rep* 2018;8:1199 CrossRef Medline
12. Tysnes BB, Mahesparan R. **Biological mechanisms of glioma invasion and potential therapeutic targets**. *J Neurooncol* 2001;53:129–47 CrossRef Medline
13. Zetterling M, Roodakker KR, Berntsson SG, et al. **Extension of diffuse low-grade gliomas beyond radiological borders as shown by the coregistration of histopathological and magnetic resonance imaging data**. *J Neurosurg* 2016;125:1155–66 CrossRef Medline
14. Barajas RF Jr, Hodgson JG, Chang JS, et al. **Glioblastoma multiforme regional genetic and cellular expression patterns: influence on anatomic and physiologic MR imaging**. *Radiology* 2010;254:564–76 CrossRef Medline
15. Ellingson BM, Malkin MG, Rand SD, et al. **Validation of functional diffusion maps (fDMs) as a biomarker for human glioma cellularity**. *J Magn Reson Imaging* 2010;31:538–48 CrossRef Medline
16. Basser PJ, Pierpaoli C. **Microstructural and physiological features of tissues elucidated by quantitative-diffusion-tensor MRI**. *J Magn Reson B* 1996;111:209–19 CrossRef Medline
17. Price SJ, Burnet NG, Donovan T, et al. **Diffusion tensor imaging of brain tumours at 3T: a potential tool for assessing white matter tract invasion?** *Clin Radiol* 2003;58:455–62 CrossRef Medline
18. Inglese M, Brown S, Johnson G, et al. **Whole-arain N-acetylaspartate spectroscopy and diffusion tensor imaging in patients with newly diagnosed gliomas: a preliminary study**. *AJNR Am J Neuroradiol* 2006;27:2137–40 Medline
19. Kleihues P, Soylemezoglu F, Schäuble B, et al. **Histopathology, classification, and grading of gliomas**. *Glia* 1995;15:211–21 CrossRef Medline

20. Won YI, Chung CK, Kim CH, et al. **White matter change revealed by diffusion tensor imaging in gliomas.** *Brain Tumor Res Treat* 2016;4:100–06 CrossRef Medline

21. Jütten K, Mainz V, Gauggel S, et al. **Diffusion tensor imaging reveals microstructural heterogeneity of normal-appearing white matter and related cognitive dysfunction in glioma patients.** *Front Oncol* 2019;9:536 CrossRef Medline

22. Maudsley AA, Roy B, Gupta RK, et al. **Association of metabolite concentrations and water diffusivity in normal appearing brain tissue with glioma grade.** *J Neuroimaging* 2014;24:585–89 CrossRef Medline

23. Malaterre M. **GDCM: Grassroots DICOM Library.** https://gdcm.sourceforge.net/wiki/index.php/Main_Page. Accessed October 29, 2022

24. Bazin PL, Cuzzocreo JL, Yassa MA, et al. **Volumetric neuroimage analysis extensions for the MIPAV software package.** *J Neurosci Methods* 2007;165:111–21 CrossRef Medline

25. Jenkinson M, Bannister P, Brady M, et al. **Improved optimization for the robust and accurate linear registration and motion correction of brain images.** *Neuroimage* 2002;17:825–41 CrossRef Medline

26. Fawcett T. **An introduction to ROC analysis.** *Pattern Recognition Letters* 2006;27:861–74 CrossRef

27. Goebell E, Fiehler J, Ding XQ, et al. **Disarrangement of fiber tracts and decline of neuronal density correlate in glioma patients: a combined diffusion tensor imaging and ^{1}H-MR spectroscopy study.** *AJNR Am J Neuroradiol* 2006;27:1426–31 Medline

28. Kassubek R, Gorges M, Westhoff MA, et al. **Cerebral microstructural alterations after radiation therapy in high-grade glioma: a diffusion tensor imaging-based study.** *Front Neurol* 2017;8:286 CrossRef Medline

29. Horváth A, Perlaki G, Tóth A, et al. **Biexponential diffusion alterations in the normal-appearing white matter of glioma patients might indicate the presence of global vasogenic edema.** *J Magn Reson Imaging* 2016;44:633–41 CrossRef Medline

30. Kallenberg K, Goldmann T, Menke J, et al. **Abnormalities in the normal appearing white matter of the cerebral hemisphere contralateral to a malignant brain tumor detected by diffusion tensor imaging.** *Folia Neuropathol* 2014;52:226–33 CrossRef Medline

31. Baykara E, Gesierich B, Adam R; et al. Alzheimer's Disease Neuroimaging Initiative. **A novel imaging marker for small vessel disease based on skeletonization of white matter tracts and diffusion histograms.** *Ann Neurol* 2016;80:581–92 CrossRef Medline

32. Song SK, Sun SW, Ramsbottom MJ, et al. **Dysmyelination revealed through MRI as increased radial (but unchanged axial) diffusion of water.** *Neuroimage* 2002;17:1429–36 CrossRef Medline

33. Uh J, Merchant TE, Li Y, et al. **Differences in brainstem fiber tract response to radiation: a longitudinal diffusion tensor imaging study.** *Int J Radiat Oncol Biol Phys* 2013;86:292–97 CrossRef Medline

34. Latini F, Fahlström M, Behánõová A, et al. **The link between gliomas infiltration and white matter architecture investigated with electron microscopy and diffusion tensor imaging.** *Neuroimage Clin* 2021;31:102735 CrossRef Medline

35. Stadlbauer A, Ganslandt O, Buslei R, et al. **Gliomas: histopathologic evaluation of changes in directionality and magnitude of water diffusion at diffusion-tensor MR imaging.** *Radiology* 2006;240:803–10 CrossRef Medline

36. Deng Z, Yan Y, Zhong D, et al. **Quantitative analysis of glioma cell invasion by diffusion tensor imaging.** *J Clin Neurosci* 2010;17:1530–36 CrossRef Medline